IN-24
167898
p.32

NASA Technical Memorandum 107753

INFLUENCE OF TRANSVERSE-SHEAR AND LARGE-DEFORMATION EFFECTS ON THE LOW-SPEED IMPACT RESPONSE OF LAMINATED COMPOSITE PLATES

Damodar R. Ambur
James H. Starnes, Jr.
Chunchu B. Prasad

April 1993

NASA

National Aeronautics and
Space Administration

Langley Research Center
Hampton, Virginia 23681
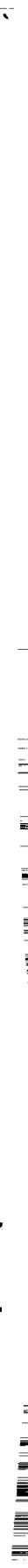
INFLUENCE OF TRANSVERSE-SHEAR AND LARGE-DEFORMATION EFFECTS ON THE LOW-SPEED IMPACT RESPONSE OF LAMINATED COMPOSITE PLATES

Damodar R. Ambur and James H. Starnes, Jr.
NASA Langley Research Center
Hampton, Virginia, USA

and

Chunchu B. Prasad
Analytical Services and Materials, Inc.
Hampton, Virginia, USA

ABSTRACT

An analytical procedure is presented for determining the transient response of simply supported, rectangular laminated composite plates subjected to impact loads from airgun-propelled or dropped-weight impactors. A first-order shear-deformation theory is included in the analysis to represent properly any local short-wave-length transient bending response. The impact force is modeled as a locally distributed load with a cosine-cosine distribution. A double Fourier series expansion and the Timoshenko small-increment method are used to determine the contact force, out-of-plane deflections, and in-plane strains and stresses at any plate location due to an impact force at any plate location. The results of experimental and analytical studies are compared for quasi-isotropic laminates. The results indicate that using the appropriate local force distribution for the locally loaded area and including transverse-shear-deformation effects in the laminated plate response analysis are important. The applicability of the present analytical procedure based on small-deformation theory is investigated by comparing analytical and experimental results for combinations of quasi-isotropic laminate thicknesses and impact energy levels. The results of this study indicate that large-deformation effects influence the response of both 24- and 32-ply laminated plates and that a geometrically nonlinear analysis is required for predicting the response accurately.

INTRODUCTION

The effect of low-speed impact damage on the compression strength of laminated composite structures has been studied extensively by many researchers over the past several years. Test data show that the compression strength of composite structures can be reduced significantly by low-speed impact damage, even if the damage is not detectable by visual inspection. Current damage-tolerance design criteria for compression-loaded composite airframe structures are related to the impact energy or to the depth of the dent in the specimen caused by the impact event. Many of the researchers who investigated the transient response of laminated composite plates used either an airgun-propelled projectile or a dropped weight to impact the specimens. The specimen support conditions were also different for many of the investigations. For an airgun impact test, a projectile of a given diameter and material is propelled at a given speed with a compressed-air apparatus to generate an impact condition that simulates the impact of an aircraft structure by runway debris and

hail stones. The dropped-weight impact test uses a weight of a given mass and material dropped from a preselected height to generate an impact condition that simulates the impact of the structure by a dropped tool. While the results of these studies all indicate that low-speed impact damage can degrade the compression strength of composite structures, there are enough differences in the results to indicate that a consistent analytical representation of the response of a composite structure to low-speed impact by a projectile or impactor is still needed. A consistent analytical representation of the response of a composite structure impacted by a low-speed impactor and the resulting initiation of damage in that structure should account for different structural, impactor and laminate parameters. These parameters include impactor mass, size and speed; specimen or target geometry, materials, laminate stacking sequence, and boundary or support conditions; and the relative magnitudes of the impactor and target masses. Earlier analytical studies that were correlated with experimental results either focused on composite structures that were impacted by a relatively large mass at low impact speeds (e.g., refs. 1-5) or on composite structures that were impacted by a relatively small mass at high impact speeds (e.g., ref. 6).

In the present paper, an analysis procedure is presented for determining the impact response of composite laminated plates. This procedure is general enough to include all of the significant structural and impactor parameters. A first-order shear-deformation theory is used in the analysis to represent properly any local short-wavelength bending transient response phenomena that may occur. The impact force has been idealized as a load that is locally distributed over a small area of the plate with a cosine-cosine distribution. The size of the loaded area is determined by an iterative procedure that accounts for the changes in the contact area between the impactor and the plate as the dynamic response of the plate develops. The contact force, out-of-plane deflections, and in-plane stresses and strains at any plate location due to an impact force at any plate location are determined using a Fourier expansion and the Timoshenko small-increment method. The analytical results are compared with experimental data for $[45/0/-45/90]_{ns}$ quasi-isotropic laminates made from a graphite-epoxy material system and subjected to low-speed impact by both airgun-propelled and dropped-weight impactors. The influence of transverse-shear deformation on the plate response is discussed for the two types of impactors. The effect of large deformations on the response of 24-, 32- and 48-ply plates with two different types of boundary conditions is also discussed.

THEORY

Governing Equations

The plate equations given by Whitney and Pagano (ref. 7) with first-order shear-deformation theory are used for the present analysis. This first-order shear-deformation theory accounts for transverse-shear deformations which can be significant for impact problems. It has been shown by Sun and Lai (ref. 8) that the first-order theory is adequate for describing a transient wave propagating in an anisotropic plate subjected to an impulsive load. The transient displacement field is assumed to be of the form

$$u = u^0(x,y,t) + z\psi_x(x,y,t)$$

$$v = v^0(x,y,t) + z\psi_y(x,y,t) \tag{1}$$

$$w = w(x,y,t)$$

where u^0, v^0 and w denote displacements of a point (x,y) in the plate mid-plane and ψ_x and ψ_y are the rotations of the normals to the mid-plane about the y and x axes, respectively (see Fig. 1). Reducing the equations of motion given in reference 7 to their specially orthotropic form and adding the uniform initial stress resultants N_x^0 and N_y^0 and the foundation stiffness K as discussed in reference 2 results in the equations

$$kA_{55}\psi_{x,x} + (kA_{55}+N_x^0)\, w_{,xx} + kA_{44}\psi_{y,y}$$
$$+ (kA_{44}+N_y^0)\, w_{,yy} + p_z + Kw = P\ddot{w}$$

$$D_{11}\psi_{x,xx} + D_{66}\,\psi_{x,yy} + (D_{12}+D_{66})\psi_{y,xy}$$
$$-kA_{55}\psi_x - kA_{55}w_{,x} = I\ddot{\psi}_x \tag{2}$$

$$(D_{12}+D_{66})\psi_{x,xy} + D_{66}\psi_{y,xx} + D_{22}\,\psi_{y,yy}$$
$$-kA_{44}\psi_y - kA_{44}w_{,y} = I\ddot{\psi}_y$$

where differentiation with respect to time t is denoted by a dot and differentiation with respect to x or y is denoted by a comma. The distributed load p_z is given by Sun and Whitney (ref. 9). The shear correction factor k is taken to be equal to $\pi^2/12$ (ref.7). The stiffnesses A_{ij} and D_{ij} and the inertias P and I are given by

$$(A_{ij}, D_{ij}) = \int_{-h/2}^{h/2} Q_{ij}(1, z^2)dz \qquad i,j=1,2,6$$

$$A_{ij} = \int_{-h/2}^{h/2} C_{ij}dz \qquad i,j=4,5 \tag{3}$$

$$(P, I) = \int_{-h/2}^{h/2} \rho(1, z^2)dz$$

where Q_{ij} are plane-stress reduced stiffnesses and C_{ij} are transverse shear stiffnesses as defined in reference 7.

A simply supported, rectangular laminated plate of uniform thickness h, length a and width b with a locally loaded area as shown in Fig. 1 is analyzed in the present study. The boundary conditions for the analysis are given by

$$w = \psi_{x,x} = 0 \qquad \text{at } x = 0, a$$

$$w = \psi_{y,y} = 0 \qquad \text{at } y = 0, b \tag{4}$$

Dynamic Loading

The general solution for the harmonic vibrations which satisfy the boundary conditions are given in reference 2 and can be expressed as

$$w(x,y,t) = W_{mn} \sin \left(\frac{m\pi x}{a}\right) \sin \left(\frac{n\pi y}{b}\right) e^{i\omega t}$$

$$\psi_x (x,y,t) = X_{mn} \cos \left(\frac{m\pi x}{a}\right) \sin \left(\frac{n\pi y}{b}\right) e^{i\omega t} \tag{5}$$

$$\psi_y (x,y,t) = Y_{mn} \sin \left(\frac{m\pi x}{a}\right) \cos \left(\frac{n\pi y}{b}\right) e^{i\omega t}$$

The contribution of the rotatory inertia terms is small and can be neglected. With this assumption, substituting equation 5 into equation 2 yields

$$[L_{ij}] \begin{bmatrix} W_{mn} \\ X_{mn} \\ Y_{mn} \end{bmatrix} = [0] \tag{6}$$

where the symmetric coefficient matrix L_{ij} is given by

$$L_{11} = (kA_{55}+N_x^0)(\frac{m\pi}{a})^2 + (kA_{44}+N_y^0)(\frac{n\pi}{b})^2 - K - \omega_{mn}^2 P$$

$$L_{12} = kA_{55} (\frac{m\pi}{a})$$

$$L_{13} = kA_{44} (\frac{n\pi}{b})$$

$$L_{22} = D_{11} (\frac{m\pi}{a})^2 + D_{66} (\frac{n\pi}{b})^2 + kA_{55} \tag{7}$$

$$L_{23} = (D_{12} + D_{66}) \left(\frac{m\pi}{a}\right) \left(\frac{n\pi}{b}\right)$$

$$L_{33} = D_{66} \left(\frac{m\pi}{a}\right)^2 + D_{22} \left(\frac{n\pi}{b}\right)^2 + kA_{44}$$

The natural frequencies ω_{mn} for the (m,n) free vibration modes of the plate are obtained by setting the determinant of the coefficient matrix L_{ij} equal to zero. The eigenvectors associated with the natural frequencies are given by

$$X_{mn} = \frac{(L_{13} L_{23} - L_{12} L_{33})}{(L_{22} L_{33} - L_{23}^2)} W_{mn}$$

$$Y_{mn} = \frac{(L_{12} L_{23} - L_{13} L_{22})}{(L_{22} L_{33} - L_{23}^2)} W_{mn} \tag{8}$$

when normalized by W_{mn}.

The dynamic response of the plate due to an impact load is transient in nature. The solutions to the equations of motion can be separated into a function of position and a function of time and expressed as (see ref. 2)

$$w(x,y,t) = \sum_{m=1}^{\infty} \sum_{n=1}^{\infty} W_{mn} \sin\left(\frac{m\pi x}{a}\right) \sin\left(\frac{n\pi y}{b}\right) T_{mn}(t)$$

$$\psi_x(x,y,t) = \sum_{m=1}^{\infty} \sum_{n=1}^{\infty} X_{mn} \cos\left(\frac{m\pi x}{a}\right) \sin\left(\frac{n\pi y}{b}\right) T_{mn}(t) \tag{9}$$

$$\psi_y(x,y,t) = \sum_{m=1}^{\infty} \sum_{n=1}^{\infty} Y_{mn} \sin\left(\frac{m\pi x}{a}\right) \cos\left(\frac{n\pi y}{b}\right) T_{mn}(t)$$

where $T_{mn}(t)$ is a time dependent generalized coordinate. Assuming that the distributed loads can be expanded into generalized forces $Q_{mn}(t)$, the resulting equation of motion can be expressed as (see ref. 2)

$$\ddot{T}_{mn}(t) + \omega_{mn}^2 T_{mn}(t) = Q_{mn}(t) \tag{10}$$

For zero initial displacement and velocity, the solution to equation (10) is given by

$$T_{mn}(t) = \frac{1}{\omega_{mn}} \int_0^t Q_{mn}(\tau) \sin \omega_{mn}(t-\tau) \, d\tau \qquad (11)$$

For cases where the rotatory inertia I can be neglected, relatively simple expressions can be developed for $w(x,y,t)$, $\psi_x(x,y,t)$ and $\psi_y(x,y,t)$. If $I = 0$, the generalized force $Q_{mn}(t)$ can be expressed as

$$Q_{mn}(t) = \frac{4}{PabW_{mn}} \int_0^a \int_0^b P_z(x,y,t) \sin\left(\frac{m\pi x}{a}\right) \sin\left(\frac{n\pi y}{b}\right) dx \, dy \qquad (12)$$

The relationship between the generalized force and the Fourier coefficients q_{mn} for a static load is given by (see ref. 2)

$$Q_{mn}(t) = \left(\frac{q_{mn}}{PW_{mn}}\right) \qquad (13)$$

The coefficients q_{mn} for the Fourier series representation of the load can be determined from

$$q_{mn} = \frac{4}{ab} \int_0^a \int_0^b p(x,y) \sin\left(\frac{m\pi x}{a}\right) \sin\left(\frac{n\pi y}{b}\right) dx \, dy \qquad (14)$$

For a concentrated load located at any arbitrary point (ξ, η), the coefficients q_{mn} are given by

$$q_{mn} = \frac{4P_z}{ab} \sin\left(\frac{m\pi \xi}{a}\right) \sin\left(\frac{n\pi \eta}{b}\right) \qquad (15)$$

where P_z is the total load. In reference 1, an impact force on a plate is modeled as a concentrated load acting at the center of the plate. This model results in a contact force that is applied over an infinitesimal area, which means that the normal shear force at the center of the impact area will be unbounded. The impact force can be modeled so that the contact force due to the impact is applied uniformly over a small, but finite, area. For such a loading condition, which is distributed over a rectangular area uv with its center at any arbitrary point (ξ, η) as shown in Figure 1, the coefficients q_{mn} are given by

$$q_{mn} = \frac{16 P_z}{\pi^2 mnuv} \sin\left(\frac{m\pi \xi}{a}\right) \sin\left(\frac{n\pi \eta}{b}\right) \sin\left(\frac{m\pi u}{2a}\right) \sin\left(\frac{n\pi v}{2b}\right) \qquad (16)$$

If the impact force is modeled to have a cosine-cosine distribution over the rectangular area uv as shown in Fig. 1, then the q_{mn} are given by

$$q_{mn} = \frac{4P_z \sin\left(\frac{m\pi\xi}{a}\right) \sin\left(\frac{n\pi\eta}{b}\right) \cos\left(\frac{m\pi u}{2a}\right) \cos\left(\frac{n\pi v}{2b}\right)}{abu2v2\left(\frac{m}{a}-\frac{1}{u}\right)\left(\frac{m}{a}+\frac{1}{u}\right)\left(\frac{n}{b}-\frac{1}{v}\right)\left(\frac{n}{b}+\frac{1}{v}\right)} \qquad \frac{m}{a} \neq \frac{1}{u}, \frac{n}{b} \neq \frac{1}{v}$$

(17)

$$q_{mn} = 0 \qquad \frac{m}{a} = \frac{1}{u}, \frac{n}{b} = \frac{1}{v}$$

Using equation (13) with equations (5), (8), (9) and (11) results in expressions for the deformations of the plate subjected to transient impact loads which are given by

$$w(x,y,t) = \frac{1}{P}\sum_{m=1}^{\infty}\sum_{n=1}^{\infty}\frac{q_{mn}\sin\left(\frac{m\pi x}{a}\right)\sin\left(\frac{n\pi y}{b}\right)}{\omega_{mn}}\int_0^t F(\tau)\sin\omega_{mn}(t-\tau)\,d\tau \qquad (18a)$$

$$\psi_x(x,y,t) = \frac{1}{P}\sum_{m=1}^{\infty}\sum_{n=1}^{\infty}\left(\frac{L_{13}L_{23}-L_{12}L_{33}}{L_{22}L_{33}-L_{23}^2}\right)\frac{q_{mn}\cos\left(\frac{m\pi x}{a}\right)\sin\left(\frac{n\pi y}{b}\right)}{\omega_{mn}}$$

$$X\int_0^t F(\tau)\sin\omega_{mn}(t-\tau)\,d\tau \qquad (18b)$$

$$\psi_y(x,y,t) = \frac{1}{P}\sum_{m=1}^{\infty}\sum_{n=1}^{\infty}\left(\frac{L_{12}L_{23}-L_{13}L_{22}}{L_{22}L_{33}-L_{23}^2}\right)\frac{q_{mn}\sin\left(\frac{m\pi x}{a}\right)\cos\left(\frac{n\pi y}{b}\right)}{\omega_{mn}}$$

$$X\int_0^t F(\tau)\sin\omega_{mn}(t-\tau)\,d\tau \qquad (18c)$$

The bending strains $\varepsilon_x, \varepsilon_y$ and γ_{xy} and the normal shear forces Q_x and Q_y at any point on the plate can be calculated using equations (18) and kinematic relations.

Impact Load

By computing the impact force from the deceleration of the impactor mass, the response of a rectangular plate subjected to an impact load can be obtained. By assuming that the vibration of the striking mass can be neglected, Timoshenko (ref. 10)

obtained the fundamental integral equation of motion for a rigid impact between a mass and a beam as

$$v_0 t - \frac{1}{m_2} \int_0^t dt \int_0^t F\, dt = w_1(c,t) \tag{19}$$

In the above equation, v_0 is the initial velocity of the impactor, m_2 is the mass of the impactor, $w_1(c,t)$ is the transient response of the beam at the impact point as a function of time and F is the contact force. Goldsmith (ref. 11) extended equation (19) to include the effect of a flexible impactor to give

$$\alpha = w_2 - w_1(c,t) = v_0 t - \frac{1}{m_2} \int_0^t dt \int_0^t F\, dt - w_1(c,t) \tag{20}$$

where the relative approach α is the distance that the impactor and the target approach one another because of local compression at the point of impact, w_2 is the displacement of the impactor and $w_1(c,t)$ is the deflection of the structure at the contact point c as shown in Figure 2. The impact force F and the relative approach or contact deformation α are related by the Hertz law for the impact of two bodies of revolution which is given by

$$F = s\, \alpha^{3/2} \tag{21}$$

Substituting equation (21) into equation (20) results in

$$\left[\frac{F}{s}\right]^{2/3} = v_0 t - \frac{1}{m_2} \int_0^t dt \int_0^t F\, dt - w_1(c,t) \tag{22}$$

where s is the contact stiffness parameter, which depends on the material and geometric properties of the plate and the impactor and is given by

$$s = \frac{4 \sqrt{R_1}}{3\pi (K_1 + K_2)} \tag{23}$$

where R_1 is the radius of the spherical indenter or impactor. If the impactor and the target are isotropic, the parameters K_1 and K_2 are given by

$$K_1 = \frac{1 - v_1^2}{\pi E_1}; \quad K_2 = \frac{1 - v_2^2}{\pi E_2} \tag{24}$$

where E_i and v_i represent the Young's moduli and Poisson's ratios, respectively, and the subscripts 1 and 2 refer to impactor and target, respectively. If the target is transversely isotropic, then K_2 is given by (see ref. 12)

$$K_2 = \frac{\sqrt{A_{22}}}{2\pi\sqrt{G_{zr}}\,(A_{11}\,A_{22} - A_{12}{}^2)}\left\{(\sqrt{A_{11}\,A_{22}} + G_{zr})^2 - (A_{12} + G_{zr})^2\right\}^{1/2} \tag{25}$$

where

$$A_{11} = E_z\,(1 - v_r)\beta; \quad A_{12} = E_r\,v_{zr}\,\beta$$

$$A_{22} = \frac{E_r\beta(1 - v_{zr}{}^2\,\delta)}{(1 + v_r)}; \quad \beta = \frac{1}{(1 - v_r - 2\,v_{zr}{}^2\,\delta)}; \quad \delta = \frac{E_r}{E_z} \tag{26}$$

and the symbols E_i, G_{ij} and v_{ij} represent the Young's moduli, shear modulus and Poisson's ratios of the target, respectively. Subscripts r and z refer to the radial and thickness directions, respectively, and z refers to the direction of the impact. Thus, v_r is the in-plane Poisson's ratio.

For the case where the impact force is modeled as a cosine-cosine distributed load over a local rectangular area of size uv, the transient response $w(x,y,t)$ is given by

$$w(x,y,t) = \frac{4}{m_1 u^2 v^2}\sum_{m=1}^{\infty}\sum_{n=1}^{\infty}\frac{\sin\left(\frac{m\pi\xi}{a}\right)\sin\left(\frac{n\pi\eta}{b}\right)}{\omega_{mn}}$$

$$X\frac{\cos\left(\frac{m\pi u}{2a}\right)\cos\left(\frac{n\pi v}{2b}\right)\sin\left(\frac{m\pi x}{a}\right)\sin\left(\frac{n\pi y}{b}\right)}{\left(\frac{m}{a} - \frac{1}{u}\right)\left(\frac{m}{a} + \frac{1}{u}\right)\left(\frac{n}{b} - \frac{1}{v}\right)\left(\frac{n}{b} + \frac{1}{v}\right)}$$

$$X\int_0^t F(\tau)\sin\omega_{mn}(t - \tau)\,d\tau \tag{27}$$

where m_1 is the mass of the plate. Substituting equation (27) into equation (22) results in a single nonlinear integral equation in terms of the contact force F between the plate and the impactor

$$\left[\frac{F}{s}\right]^{2/3} = v_0 t - \frac{1}{m_2} \int_0^t dt \int_0^t F\, dt - \frac{4}{m_1 u^2 v^2} \sum_{m=1}^{\infty} \sum_{n=1}^{\infty} \frac{\sin\left(\frac{m\pi\xi}{a}\right) \sin\left(\frac{n\pi\eta}{b}\right)}{\omega_{mn}}$$

$$X \frac{\sin\left(\frac{m\pi x}{a}\right) \sin\left(\frac{n\pi y}{b}\right) \cos\left(\frac{m\pi u}{2a}\right) \cos\left(\frac{n\pi v}{2b}\right)}{\left(\frac{m}{a}-\frac{1}{u}\right)\left(\frac{m}{a}+\frac{1}{u}\right)\left(\frac{n}{b}-\frac{1}{v}\right)\left(\frac{n}{b}+\frac{1}{v}\right)}$$

$$X \int_0^t F(\tau) \sin \omega_{mn}(t-\tau)\, d\tau \tag{28}$$

which is solved numerically by applying the small-increment method suggested by Timoshenko (ref. 10). The finite difference procedure given by Chou and Mortimer (ref. 13) has been modified and incorporated into a computer code with the Timoshenko small-increment method to conduct the analyses for the current study.

Size of Area for Locally Distributed Load

The analysis used in the current study is general enough to represent load cases where the load is modeled as a point load, as a local load distributed uniformly over a rectangular area of size uv, or as a local load distributed over a rectangular area of size uv by a cosine-cosine function. The center of the areas of the distributed loads can be located at any arbitrary point. Since the model with the cosine-cosine load distribution more closely represents the physical problem and, hence, will provide a better comparison between analytical and experimental results, all results presented in the current paper are based on the local cosine-cosine load distribution.

Most previous investigators represented the impact force in their analytical models by a local load that is uniformly distributed over a square with side dimensions equal to the radius of the impactor. This approximation is not a true representation of the size of the area over which the actual load is distributed, and leads to errors in strains in the vicinity of the impact site. Hence, in the present study, the size of the loaded area uv is determined by using an iterative approach. Since only spherical impactors are used in the experimental study, it is assumed that the loaded area can be approximated by a square, i.e., u = v. In this iterative approach, an initial analytical iteration is conducted with u and v values corresponding to the footprint of a given impactor on the target with no applied contact force. The maximum value of the contact force and the corresponding value of the relative approach α is estimated for these initial values of u and v. The size of the loaded area for the next iteration is calculated from this maximum value of α using

$$u = v = 2\sqrt{\alpha_{max}(2R_1 - \alpha_{max})} \tag{29}$$

This procedure is continued until converged values for u and v are obtained. The final calculations for the contact force, deflections and stresses use the final values of u and v. Converged values of u and v are generally obtained within three or four iterations.

Convergence Studies

It was shown in reference 14 that a relatively large number of modes is required to obtain converged surface strain values for a point that corresponds to the impact site on the plate surface opposite to the impacted surface. A convergence study was conducted for the present investigation using the dimensions of the test specimens and arbitrary impact site and strain locations to account for variations in the test parameters. The results of this convergence study suggest that using 150 terms in the Fourier expansion in the x direction and 300 terms in the Fourier expansion in the y direction will ensure converged strain results in the analysis. All analysis results presented in the present paper are based on values of m equal to 150 and n equal to 300 for the modes included in the solution. A value of 1 μsec is used for the time increment in the transient analysis for most of the analytical results for the airgun impact studies. A value of 10 μsec is used for the time increment in the transient analysis for the dropped-weight impact studies.

EXPERIMENTS

Test Specimens

The specimens tested in this investigation were fabricated from commercially available unidirectional graphite fiber tapes preimpregnated with an epoxy resin. Hercules, Inc. AS4 graphite fibers and Hercules, Inc. 3502 epoxy resin were used in this study. The mechanical properties for the AS4/3502 graphite-epoxy material system are as follows: longitudinal extensional modulus, E_1=20.0 Msi; transverse extensional modulus, E_2=1.30 Msi; in-plane shear modulus, G_{12}=0.87 Msi; transverse shear moduli, G_{23}=0.51 Msi and G_{13}=0.87 Msi; and major Poisson's ratio, v_{12}=0.3. Unidirectional tapes were laid up to form 24-, 32- and 48-ply $[45/0/-45/90]_{ns}$ quasi-isotropic laminated plates and cured in an autoclave using the resin manufacturer's recommended procedure. The resulting plates were ultrasonically inspected to establish specimen quality and then machined into 5-in.-wide by 10-in.-long rectangular specimens. The identification of commercial products in the present paper is intended to describe adequately the test specimens and does not constitute endorsement, expressed or implied, by the National Aeronautics and Space Administration.

Apparatus and Tests

Knife-edge supports were used to provide simply supported boundary conditions for the test specimens. The knife-edge supports were attached to each edge of the specimens at locations 0.25 inches in from each edge. Each specimen was impacted on one surface at the specimen center by either an airgun-propelled or a dropped-weight impactor. The airgun used in this study is based on the airgun described in Reference 15. The airgun-propelled impactors were 0.5-in.-diameter aluminum or

steel balls that were propelled at the specimens with a given speed. The dropped-weight impactor consisted of a 2.6-lb dropped-weight assembly with an instrumented tup and 0.5- and 1.0-in.-diameter steel impactor tips. For the dropped-weight impact tests, the dropped-weight assembly was raised to a desired height and then released to impact the specimen. All specimens were instrumented with electrical resistance strain gages mounted on the specimen surface opposite to the surface to be impacted as shown in Figure 3. Force and strain gage data were recorded using a digital storage oscilloscope.

RESULTS AND DISCUSSION

The analytical and experimental results of this study are presented and compared in this section. Analytical results are presented for 4.5-in.-wide by 9.5-in.-long plate models since the knife-edge supports for the test specimens are located 0.25 inches in from the actual specimen boundaries. Thus, for a perfect central impact, the coordinates for the impact site are $x = 2.5$ in. and $y = 5.0$ in. as shown in Figure 1. The analytical formulation presented in a previous section is for specially orthotropic plates where the coupling stiffnesses D_{16} and D_{26} are assumed to be equal to zero. The D_{16} and D_{26} terms are not equal to zero for quasi-isotropic specimens, but they are neglected in the analysis since they are small.

Effect of Size of Area for Locally Distributed Load

As indicated in a previous section, the size of the area of the locally distributed load influences the predicted response considerably and an iterative approach has been used in the present analysis procedure to estimate the correct loaded area size. The converged value for the predicted loaded area size is verified for both the airgun-propelled and dropped-weight impact cases by comparing the predicted values with the measured values. The results for a 48-ply quasi-isotropic laminate impacted by a 0.5-in.-diameter steel impactor with increasing impact speeds are presented in Figures 4(a) and 4(b) for airgun-propelled and dropped-weight impactors, respectively. The correlation of the results is very good. The analytical and measured strain results for an airgun-propelled 0.5-in.-diameter steel ball with 2.18 ft-lb of impact energy are compared in Figure 4(c) as a function of time to illustrate the errors associated with the use of an arbitrary 0.25-in.-square loaded area size. The strain magnitudes obtained using an iteratively determined loaded area size compare very well with the experimental results for strain gage location 3 in Figure 3. The analytical results obtained with an arbitrary 0.25-in.-square loaded area size underestimates one of the strains by about 40 percent.

In-plane Strains

Controlling the trajectory of an airgun-propelled or a dropped-weight impactor well enough to strike a specimen precisely at the desired impact site has proven difficult to accomplish in the laboratory with currently available equipment. In practice, the impact site location is not necessarily at the center of the plate and the strains and deflections of interest may be at any plate location. The present analysis is capable of predicting the deflections and strains at any plate location caused by an impact event at any plate location. By providing the measured impact-site and strain-gage locations, it is possible to calculate the plate transient response. An airgun-impact

example with an off-center impact-site location is used to demonstrate this capability of the present analysis. A 0.24-in.-thick AS4/3502 graphite-epoxy plate is impacted by a 0.5-in.-diameter aluminum ball with an impact speed of 124.1 ft/sec at $x = 1.95$ in. and $y = 4.75$ in. (near strain gage 3 in Fig. 3). The corresponding experimental and analytical strain results are compared in Figure 5. The maximum strain is tensile and is measured by strain gage 3 near the impact site. The strain measured by strain gage 1, which is farthest from the impact site, is first compressive and then tensile as time increases. The strain measured by strain gage 2 has values of strain that are between the strains measured by strain gages 1 and 3. Comparing the predicted and measured strain data shown in Figure 5 indicates that the present analysis can predict the in-plane strains at any arbitrary point on the plate for off-center impact sites with reasonable accuracy.

Transverse-Shear-Deformation Effects

The longitudinal strains on the surface opposite to the point of impact for a 0.5-in.-diameter steel airgun-propelled impactor with 1.05 and 1.60 ft-lb of impact energy are shown in Figures 6(a) and 6(b), respectively, as a function of time. For the laminate subjected to 1 ft-lb of impact energy, the analytical strain results with and without transverse-shear-deformation effects coincide with one another and also with the experimental data represented by the open symbols for the first 10 μsec. The data after 10 μsec indicate that the phase of the analytical strain profiles with and without transverse-shear-deformation effects are significantly different because of the natural frequency reduction associated with including transverse-shear-deformation effects in the analysis. Although the magnitudes of the differences in strain between the experimental and analytical results with transverse-shear- deformation effects indicate a large discrepancy, the phase difference is negligible. The strain magnitudes are very sensitive to the location of the impact site, and part of this difference in strain magnitudes is attributed to the difficulty in measuring the exact impact-site location for the airgun experiments. The longitudinal strain results (strain gage 2A in Fig. 3) for a laminate subjected to an impact energy level of 1.60 ft-lb is shown in Figure 6(b) where the experimental and analytical results correlate well when transverse-shear-deformation effects are included in the analysis. The out-of-plane deflection profile corresponding to the 1.05 ft-lb impact energy level is shown in Figure 6(c). This curve corresponds to the time at which the maximum longitudinal strain occurs in the plate and indicates the local nature of the plate deflection for this impact case. Even for this relatively small impact energy level, the ratio of the deflection half-wave length λ to the plate thickness h is equal to 11. The value for the ratio λ/h decreases for increasing impact energy levels and the value of this ratio corresponding to 2.18 ft-lb of impact energy is equal to 8.1. Even for isotropic materials, transverse-shear deformations affect the results by approximately 5 percent for a λ/h ratio equal to 10 (ref. 16). The results presented above are consistent with the observation that classical plate theory is generally in error for λ/h ratios less than 20 for specially orthotropic laminates and indicate that it is important to include transverse-shear-deformation effects in the airgun impact analysis. Transverse-shear-deformation effects cannot be neglected for laminated plates subjected to impacts as was suggested in reference 6.

The longitudinal strain results for plates subjected to dropped-weight impact energy levels of 2.18 and 3.0 ft-lb are presented in Figures 6(d)-6(f). A 0.5-in.-

diameter steel impactor was used for the 2.18 ft-lb impact energy case and the strain results measured by a strain gage rosette located on the surface (see Fig. 3) opposite to the point of impact are compared with the analytical results shown in Figure 6(d) by the solid curves. These results indicate that the response due to the dropped-weight impactor occurs over a much longer time period than the response due to the airgun-propelled impactor and that transverse- shear deformations do not have a significant effect on either the magnitude or the phase of the strain response for this case. The phase is minimally affected since the impactor mass is large relative to the target mass. The axial strains for a 3.0 ft-lb dropped-weight impactor energy level associated with impactors with different impactor-tip diameters are shown in Figures 6(e) and 6(f). Transverse-shear deformations influence only the magnitude and not the phase of the response for cases with 0.5-in.- and 1-in.-diameter impactor tips suggesting that transverse-shear-deformation effects become important as the impact energy level is increased. The λ/h ratios calculated from the out-of-plane deflection curves corresponding to the 2.18 and 3.0 ft-lb impact energy levels are 16 and 15, respectively. Although these ratios are larger than the λ/h ratios for the airgun impact cases with lower impact energy levels, transverse-shear-deformation effects still appear to be important for the 3.0 ft-lb impact case. Since the results of the analysis with transverse-shear-deformation effects included provide better correlation between the analytical and experimental results for both the airgun and dropped-weight impact tests, all subsequent analytical results presented in the present paper have been determined with transverse-shear-deformation effects included. The need for including transverse-shear-deformation effects in the analysis for the specially orthotropic laminates considered in the present paper is well documented (e.g., refs. 8 and 16).

Large-Deformation Effects

Nonlinear effects associated with large deformations can influence the plate response if the out-of-plane deflections are a significant percentage of the plate thickness or if the boundary conditions restrain the in-plane deflections enough to contribute to the membrane strains. Increasing the magnitude of the impact speed can cause large deformations if the plate is thin enough. The effects of geometric nonlinearities are negligible for a simply supported 48-ply quasi-isotropic laminate subjected to either an airgun-propelled or a dropped-weight impactor if the impact energy level is less than 4.0 ft-lb, which is the threshold impact energy level for which damage is initiated in the plate. The maximum out-of-plane deflection w for such a plate subjected to an impactor with 4.0 ft-lb of impact energy is less than 0.2 times the plate thickness h for a dropped-weight impactor and is approximately 0.063 times the plate thickness for an airgun-propelled impactor. The results of the present study indicate that a dropped-weight impactor with an impact energy level below the 4.0 ft-lb threshold causes the largest out-of-plane deflection and, hence, suggest that nonlinear effects are likely to be more pronounced for a dropped-weight impact case. As a result, only dropped-weight impact cases are investigated further in the present paper. The predicted strains in the longitudinal and lateral directions for a 48-ply (0.25-in.-thick) laminate subjected to a 4.0 ft-lb dropped-weight impactor are compared with the experimental results in Figure 7(a). The correlation between the experimental and analytical results is very good. For plates that are thinner than 0.25 in., however, the applicability of the present small-deformation theory could be limited since the w/h ratio will typically be larger for the thinner plates than for the 48-ply plate and will

increase for increasing impact energy levels. To identify these limitations, a dropped-weight impact study was conducted for 24- and 32-ply quasi-isotropic laminated plates subjected to increasing impact energy levels. The results of this study for simply supported 24- and 32-ply-thick, 5-in.-wide, 10-in.-long graphite-epoxy plates are expressed in terms of the w/h ratios and presented in Figures 7(b) and 7(c) as a function of impactor speeds for impact energy levels up to 4.0 ft-lb. The w/h ratios are less than 0.7 for the 32-ply (0.166-in.-thick) specimens and are as large as 1.2 for the 24-ply (0.128-in.-thick) specimens. Large-deformation effects are expected to influence the plate response for w/h ratios greater than 0.5.

The measured and predicted longitudinal strain results for dropped-weight impact cases are presented in Figures 7(d) and 7(e) for the 24-ply specimens and in Figures 7(f) and 7(g) for the 32-ply specimens. The predicted results are represented by the curves and the measured results are represented by the symbols. For the 1.0 ft-lb impact energy case, the correlation between the predicted and measured strains is very good. As the impact energy level is increased to 2.18 ft-lb, there is a discrepancy between the measured and predicted strains for both the 24- and the 32-ply specimens. This discrepancy is due to membrane effects that influence the deflection and, hence, the in-plane strains of the plates. The value of the w/h ratio for the 2.18 ft-lb impact energy case is equal to 0.43 for the 32-ply specimen and is equal to 0.75 for the 24-ply specimen. The difference in the measured and predicted strains is approximately 13 percent for the 24-ply specimen and approximately 8 percent for the 32-ply specimen. The differences are 14.5 percent and 10 percent for the 24-ply and 32-ply laminates, respectively, for the 3.0 ft-lb impact energy case. The differences between the present small-deformation-theory results and the experimental results for the 4.0 ft-lb impact energy case are 28.5 and 22.5 percent, respectively, for the two laminates. The values of the w/h ratios for 24- and 32-ply laminates for the 4.0 ft-lb impact energy level is 1.20 and 0.68, respectively. These results indicate that, even for simply supported boundary conditions, an impact energy greater than 3.0 ft-lb would require an analysis to include large-deformation effects in order to be accurate for quasi-isotropic laminates thinner than the thickness of a 32-ply specimen.

The influence of boundary conditions on the nonlinear response of both 24- and 32-ply quasi-isotropic laminated plates has been determined experimentally. The response of plates with all four edges simply supported is compared with the response of plates with the two long sides simply supported and the two short sides clamped in Figure 8. The longitudinal strains on the surface of the plate opposite to the impact site for 24-ply specimens and for the two sets of boundary conditions are compared in Figure 8(a) for 1.0 and 2.18 ft-lb of impact energy. For the 1 ft-lb impact energy level, the maximum difference in the longitudinal strain magnitude between plates with different sets of boundary conditions is 17 percent. This difference for the 2.18 ft-lb impact energy level is 26 percent. The corresponding results for 32-ply specimens are presented in Figure 8(b). The differences in strain magnitudes for the 32-ply specimens are smaller than the differences in strain magnitudes for the 24-ply specimens. The membrane strain results from gages 2A and 2B shown in Figure 3 for the two impact energy levels are presented in Figure 8(c) for 24-ply specimens. The results indicate that the membrane strains for plates with two sides simply supported and two sides clamped are much higher than the corresponding strains for plates with all four sides simply supported. These results indicate that nonlinear effects and proper boundary conditions should be accounted for when studying the impact response of composite laminates.

CONCLUDING REMARKS

An analytical procedure has been developed for determining the transient response of simply supported, rectangular laminated composite plates subjected to low-speed impact loads and the procedure has been verified experimentally. A first-order shear-deformation theory has been used for the analysis and the impact force has been modeled as a locally distributed force with a cosine-cosine distribution. An iterative approach has been used to determine the correct size of the loaded area which is important for accurately predicting the impact response of composite plates. The analysis method presented can predict the plate response at any plate location due to an impact force applied at any plate location. Both airgun-propelled and dropped-weight impactors can be represented by the analysis.

The influence of transverse-shear deformations on plate response for an airgun-propelled impactor is to advance the phase of the impact contact force and surface strain profiles even for low impact energy levels and to affect the magnitudes of impact contact force and surface strains for higher impact energy levels. This behavior is due to the short wave lengths of the local out-of-plane deflection associated with the impact event which decrease with increasing impact energy levels. For dropped-weight impactors, only the magnitude of the response is affected by not including transverse-shear effects. The analytical results agree well with the experimental results when transverse-shear effects are included in the analysis confirming the importance of including these secondary effects when studying the impact response of composite plates.

Nonlinear effects associated with large out-of-plane deformations are pronounced for simply supported laminates that are thinner than a 32-ply laminate for impact energies that are less than the impact energy necessary to initiate damage. Large errors in the response predictions for the thinner laminates have been observed if a small-deformation theory is used for the analysis. When two opposite edges of a plate are clamped and the other two edges are simply supported, nonlinear effects are more pronounced than when all four sides are simply supported. These results indicate the need to include large-deformation effects and the appropriate boundary conditions in the analysis of composite plates in order to predict their low-speed impact response accurately.

REFERENCES

1. Sun, C. T.; and Chattopadhay, S.: Dynamic Response of Anisotropic Laminated Plates Under Initial Stress to Impact of a Mass. Journal of Applied Mechanics, Vol. 42, September 1975, pp. 693-698.

2. Dobyns, A. L.: Analysis of Simply-Supported Orthotropic Plates Subject to Static and Dynamic Loads. AIAA Journal, Vol. 19, No. 5, May 1981, pp. 642-650.

3. Ochoa, C. M.: Nondimensional Models for Low Velocity Impact of Laminated Composite Panels. Proceedings of the AIAA/ASME/ASCE/AHS 28th Structures, Structural Dynamics, and Materials Conference, Monterey, CA, April 6-8, 1987, pp. 443-447. AIAA Paper No. 87-0802.

4. Shivakumar, K. N.; Elber, W.; and Illg, W.: Prediction of Low-Velocity Impact Damage in Thin Circular Laminates. AIAA Journal, Vol. 23, No. 3, March 1985, pp. 442-449.

5. Christoforou, A. P.; and Swanson, S. R.: Analysis of Impact Response in Composite Plates. International Journal of Solids and Structures, Vol. 27, No. 2, 1991, pp. 161-170.

6. Olsson, R.: Impact Response of Orthotropic Composite Plates Predicted from a One-Parameter Differential Equation. AIAA Journal, Vol. 10, No. 6, June 1992, pp. 1587-1596.

7. Whitney, J. M.; and Pagano, N. J.: Shear Deformation in Heterogeneous Anisotropic Plates. Journal of Applied Mechanics, Transactions of the ASME, Vol. 37, December 1970, pp. 1031-1036.

8. Sun, C. T., and Lai, R. Y. S.: Exact and Approximate Analysis of Transient Wave Propagation in an Anisotropic Plate. AIAA Journal, Vol. 12, No. 10, October 1974, pp. 1415-1417.

9. Sun, C. T.; and Whitney, J. M.: Forced Vibration of Laminated Composite Plates in Cylindrical Bending. Journal of Acoustic Society of America, Vol. 55, May 1974, pp. 1003-1008.

10. Timoshenko, S. P.: Zur Frage nach der Wirkung eines Stosses auf einer Balken. Zeitschrift fur Mathematik and Physik, Vol. 62, 1913, pp. 198-209.

11. Goldsmith, W.: Impact, Edward Arnold Ltd., London, 1960.

12. Conway, H. D.; and Angew, Z.: The Pressure Distribution Between Two Elastic Bodies in Contact. Journal of Mathematics and Physics, Vol. 7, 1956, pp. 460-465.

13. Chou, P. C.; and Mortimer, R. W.: Impact Behavior of Polymeric Matrix Composite Materials. Report No. AFML-TR-76-242, Air Force Materials Laboratory, Wright-Patterson AFB, Ohio, December, 1976.

14. Qian, Y.; and Swanson, S. R.: A Comparison of Solution Techniques for Impact Response of Composite Plates. Composite Structures, Vol. 14, No. 3, 1990, pp. 177-192.

15. Starnes, J. H., Jr.; Rhodes, M. D.; and Williams, J. G.: Effect of Impact Damage and Holes on the Compressive Strength of a Graphite/Epoxy Laminate. Nondestructive Evaluation and Flaw Criticality for Composite Materials, ASTM STP 696, edited by R. B. Pipes, American Society for Testing and Materials, Philadelphia, PA, 1979, pp. 145-171.

16. Reddy, J. N.: A Refined Nonlinear Theory of Plates with Transverse Shear Deformation. International Journal of Solids and Structures, Vol. 20, No. 9/10, 1984, pp. 881-896.

Cosine load

$$p = p_0 \cos \frac{\pi}{u}(x-\xi) \cos \frac{\pi}{v}(y-\eta)$$
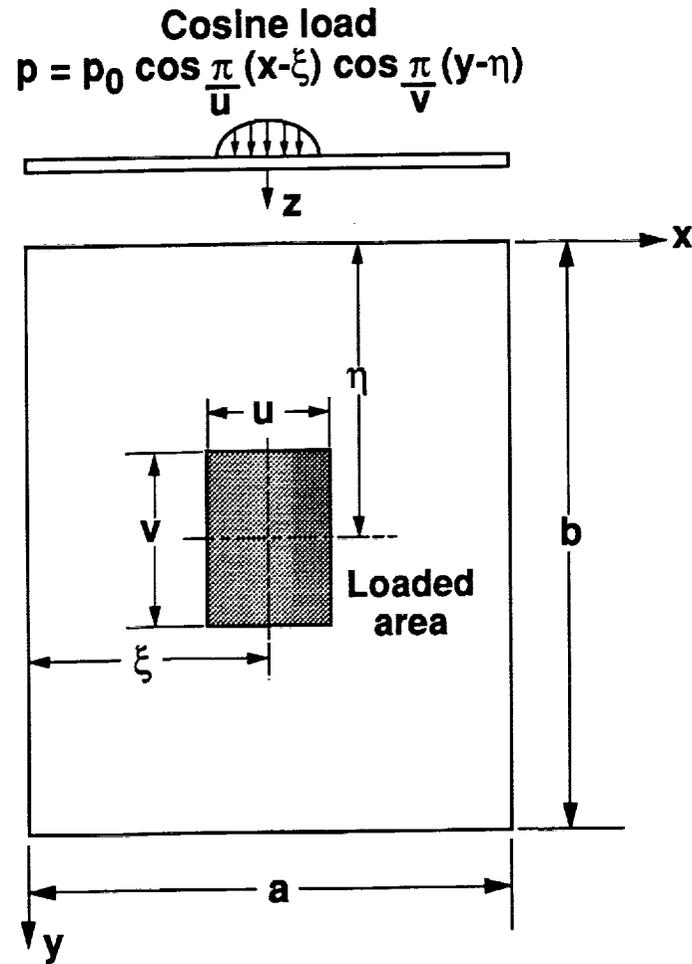
Fig. 1 Plate coordinates, and location and shape of loaded area.
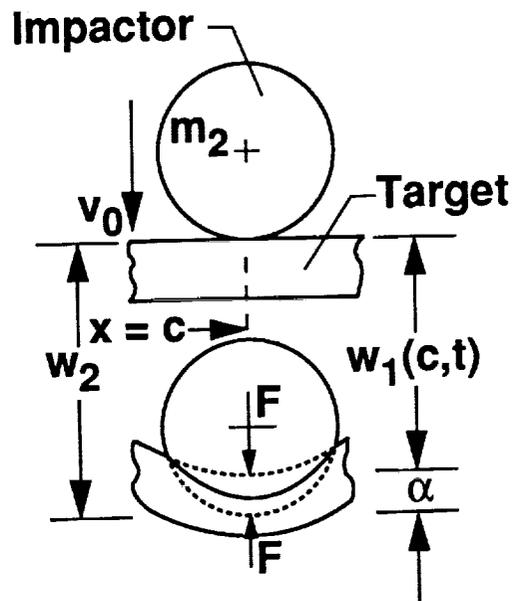
Fig. 2 Transverse impact of a spherical body with a curved contact surface.
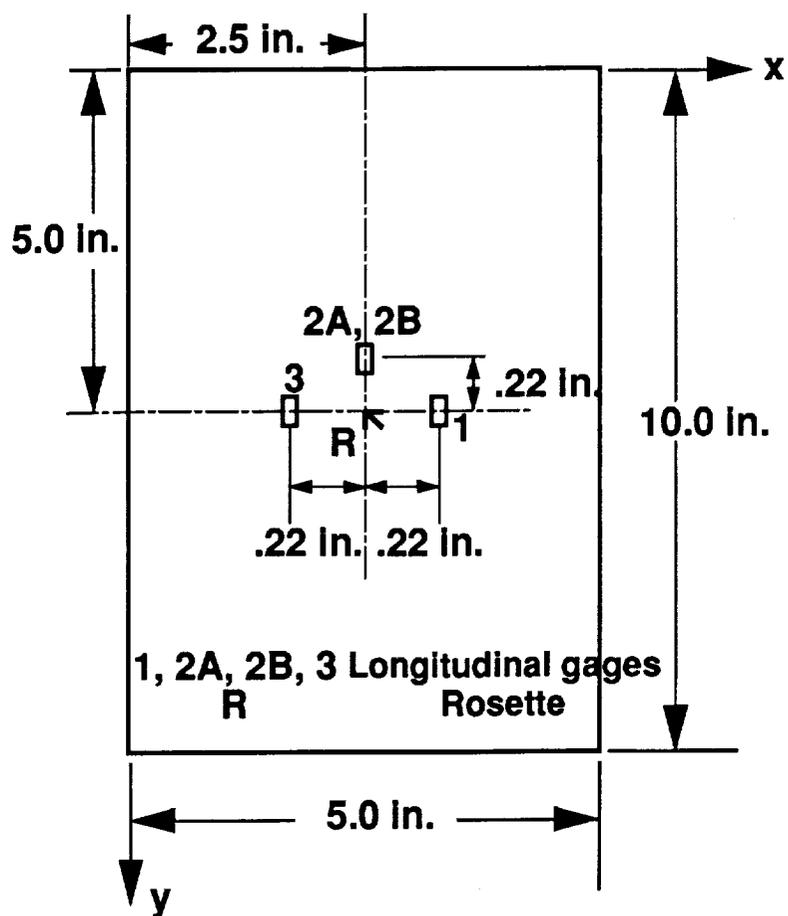
Fig. 3 Strain gage locations (all gages excepting gage 2B are located on the surface opposite to the impacted surface)
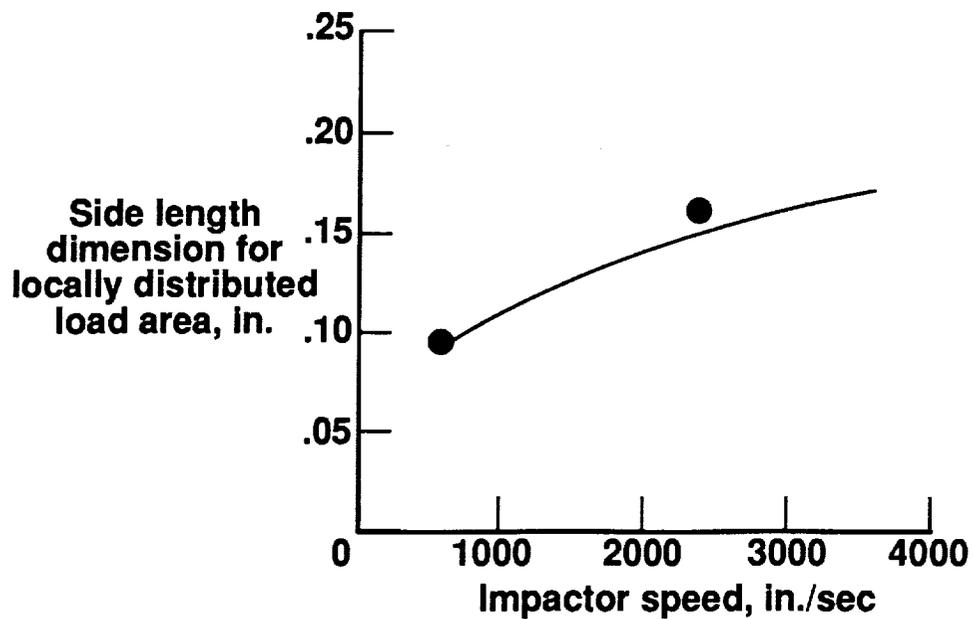
4(a) Comparison of locally distributed load area for 48-ply laminate subjected to airgun impact.

Figure 4. Comparison of locally distributed load area and its influence on the laminated plate response.
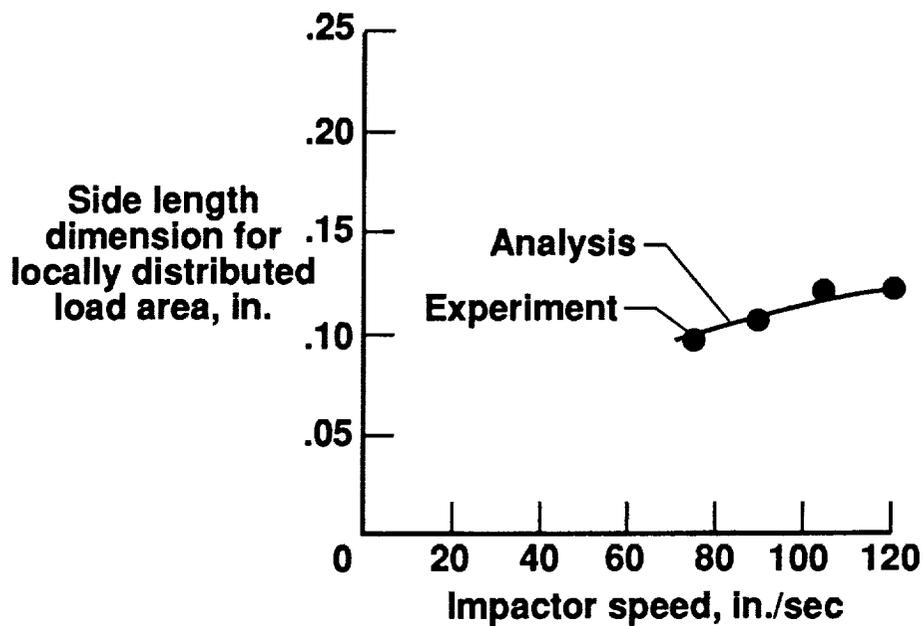
4(b) Comparison of locally distributed load area for 48-ply laminate subjected to dropped-weight impact.

Fig. 4 Continued
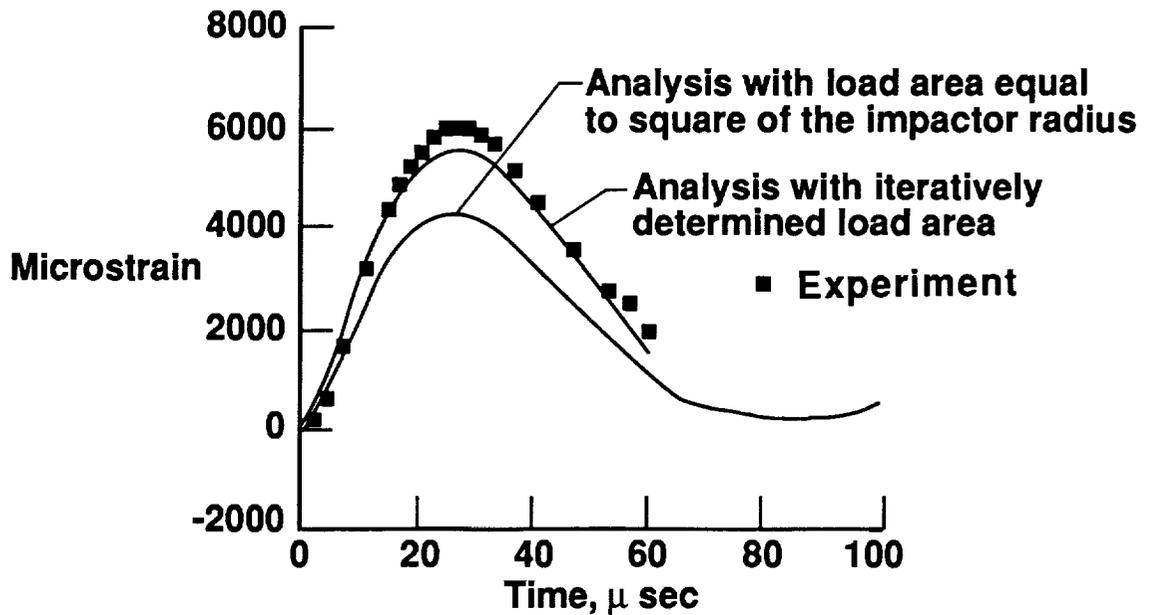
4(c) Effect of locally distributed load area on the response of a 48-ply laminate for airgun impact with 0.5-in.-diameter-steel ball.

Fig. 4 Concluded.
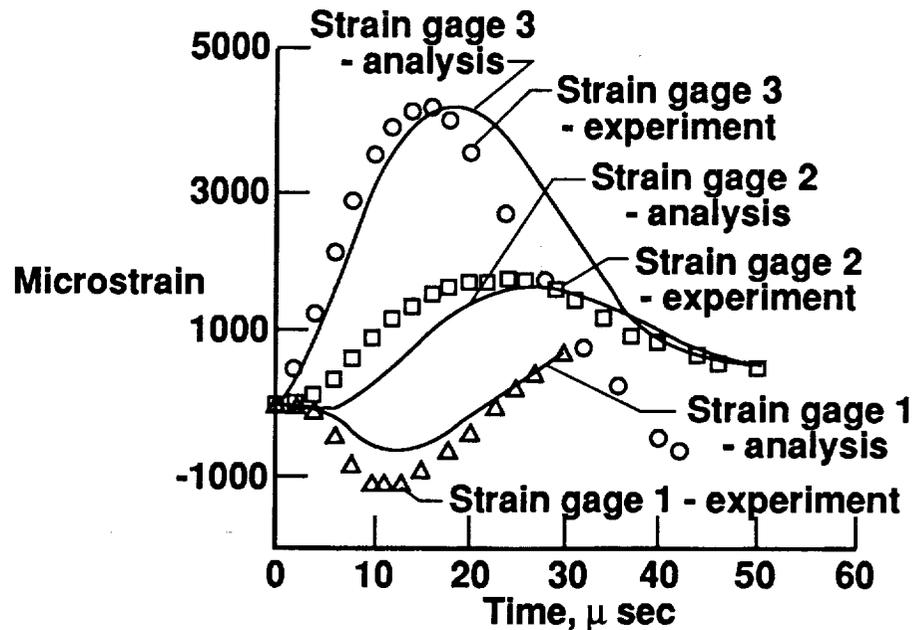
Fig. 5 Comparison of strain profiles for a 5-in.-wide by 10-in.-long graphite-epoxy plate at three locations for an off-center airgun impact with a 0.5-in.-diameter aluminum ball with 124.1 ft/sec impact speed.
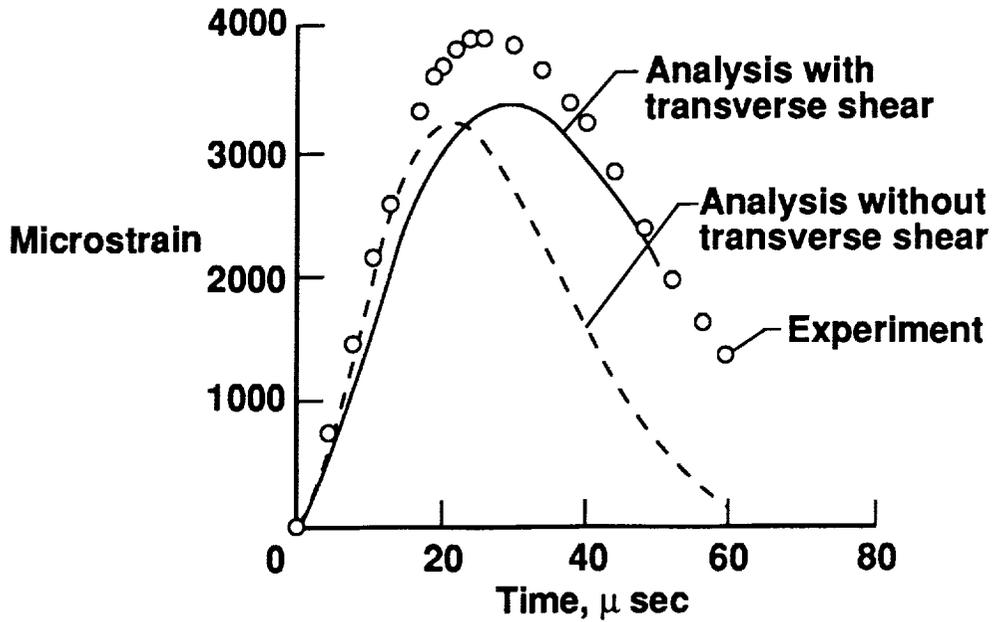
6(a) Longitudinal strain at plate center for an airgun impact with a 0.5-in.-diameter steel ball with 1.05 ft-lb impact energy.

Fig. 6 Effects of transverse-shear deformation on the response of 5-in.-wide by 10-in.-long graphite-epoxy plates subjected to lateral impact.
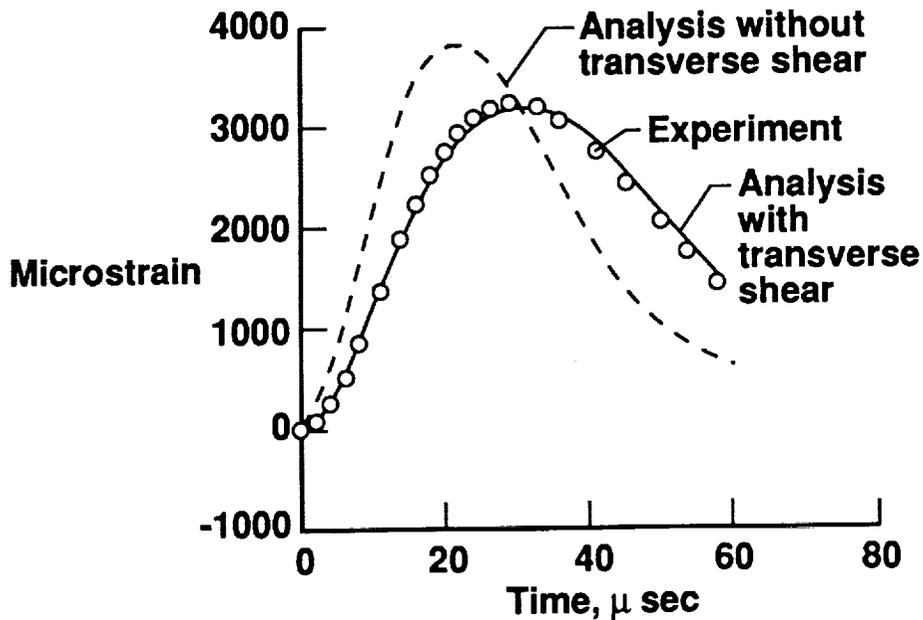
6(b) Longitudinal strain at plate center for an airgun impact with a 0.5-in.-diameter steel ball with 1.60 ft-lb of impact energy.

Fig. 6 Continued
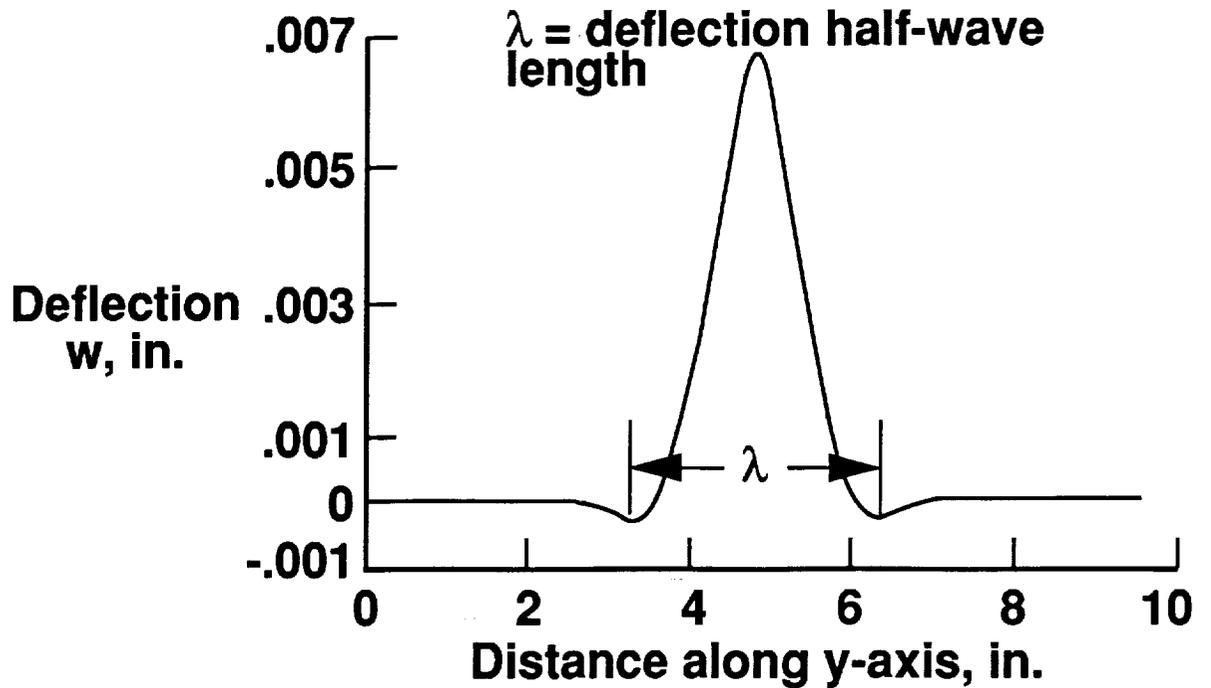
6(c) Deflection profile along y-axis at x=2.5 in. after 30 μsec for airgun impact with 1.05 ft-lb of impact energy from a 0.5-in.-diameter steel ball.
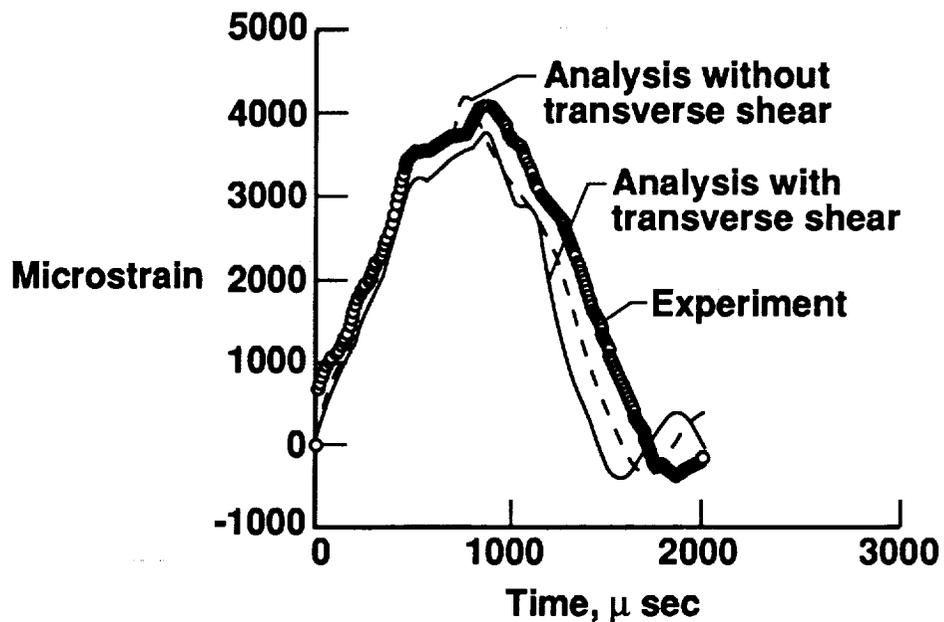
6(d) Longitudinal strain at plate center for dropped-weight impact with a 0.5-in.-diameter steel tip with 2.18 ft-lb of impact energy.

Fig. 6 Continued.
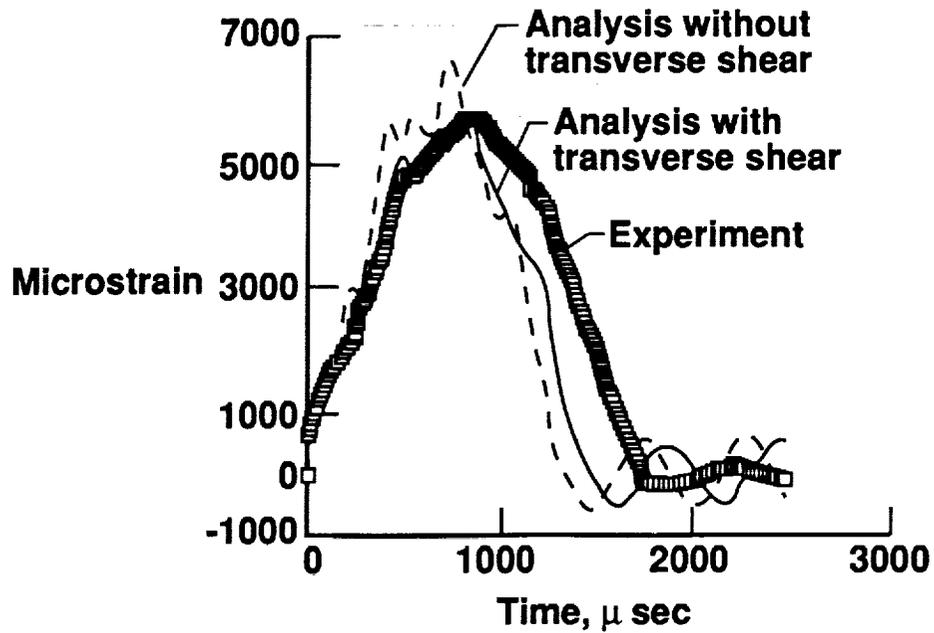
6(e) Longitudinal strain at plate center for dropped-weight impact with a 0.5-in.-diameter steel tip with 3.0 ft-lb impact energy.
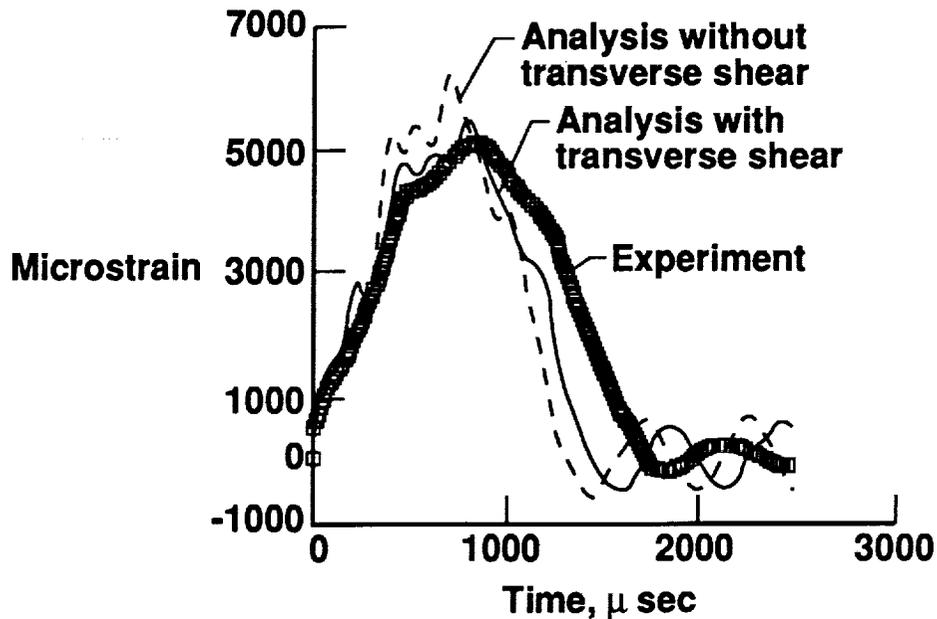
6(f) Longitudinal strain at plate center for dropped-weight impact with 1.0-in.-diameter steel tip with 3.0 ft-lb of impact energy.

Fig. 6 Concluded.
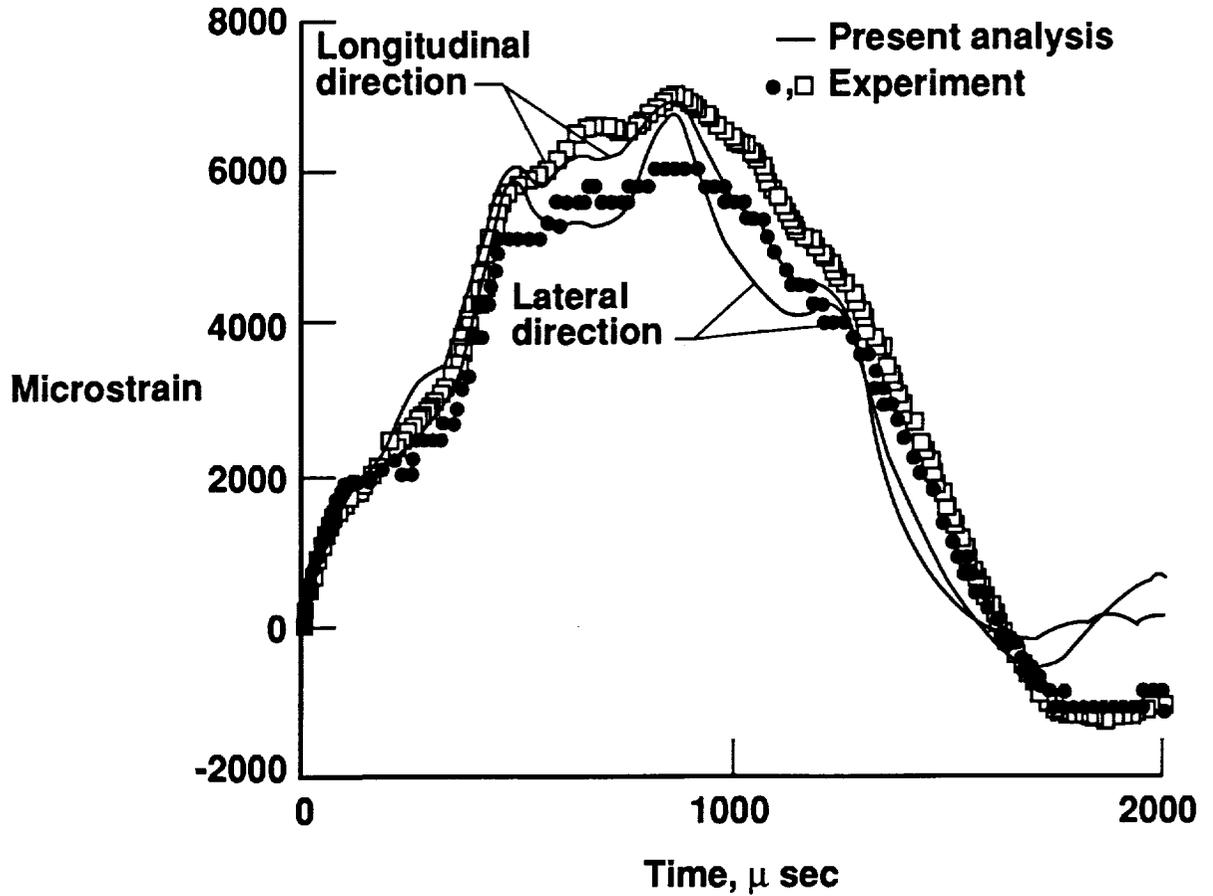
7(a) Comparison of measured strains on surface opposite to impact side in a 48-ply simply supported laminate subjected to 4.0 ft-lb dropped-weight impact.

Fig. 7 Influence of large deformations on the impact response of 5.-in.-wide and 10-in.-long laminated graphite-epoxy plates for increasing impact energy levels.
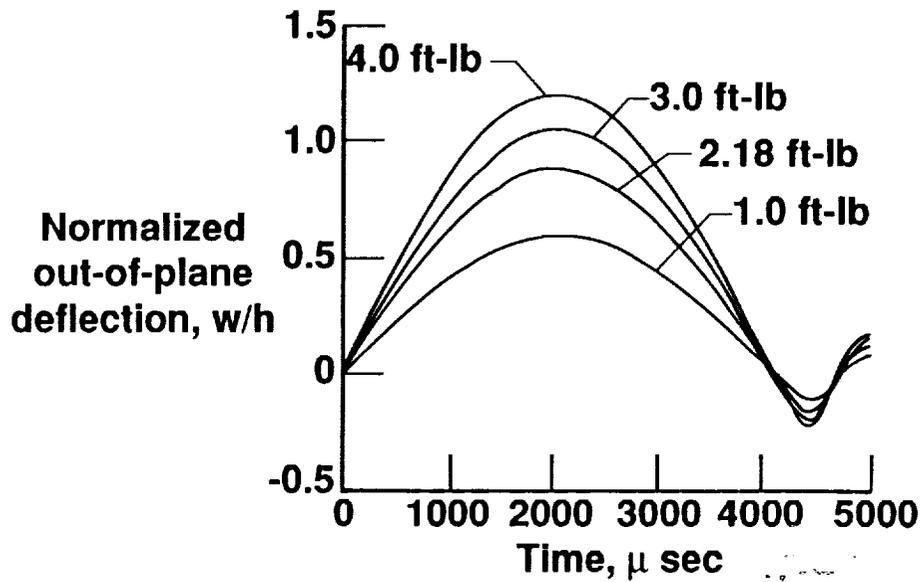
7(b) Normalized out-of-plane displacement profiles for a 24-ply simply supported
laminated plate subjected to dropped-weight impacts.
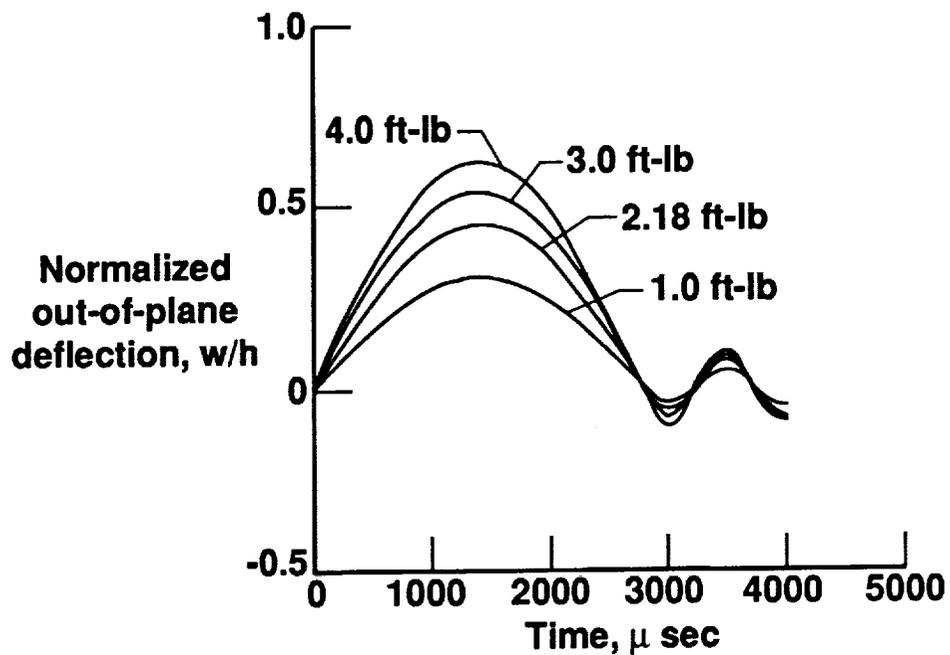
7(c) Normalized out-of-plane displacement profiles for a 32-ply simply supported
laminated plate subjected to dropped-weight impacts.

Fig. 7 Continued.
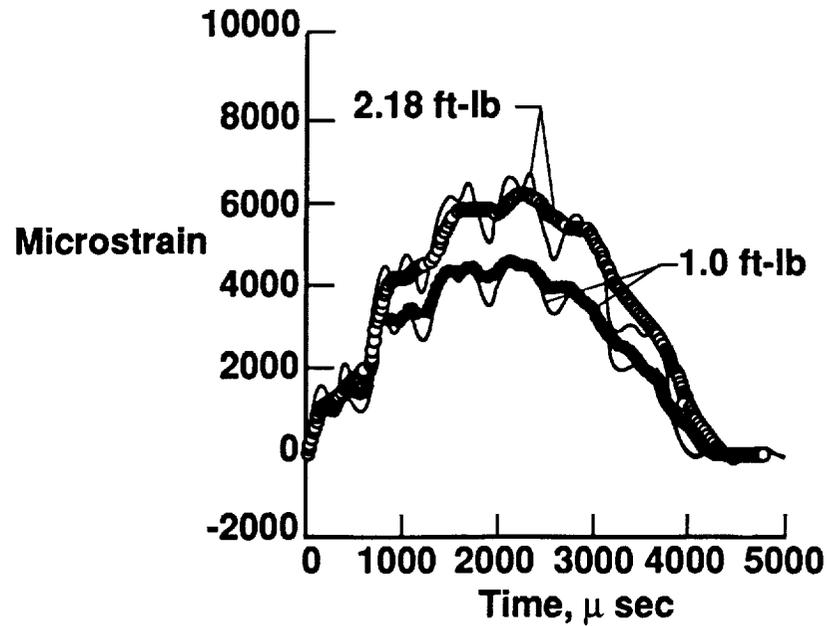
7(d) Comparison of analytical and experimental strains on surface opposite to impact side in a 24-ply simply supported laminated plate subjected to 1 and 2.18 ft-lb of dropped-weight impact.
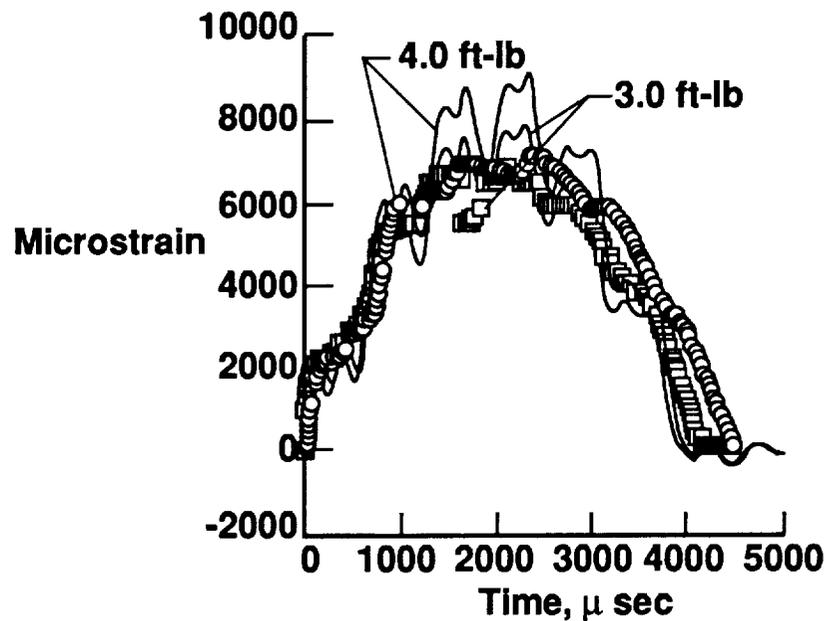
7(e) Comparison of analytical and experimental strains on surface opposite to impact side in a 24-ply simply supported laminated plate subjected to 3.0 and 4.0 ft-lb of dropped-weight impact.

Fig. 7 Continued.
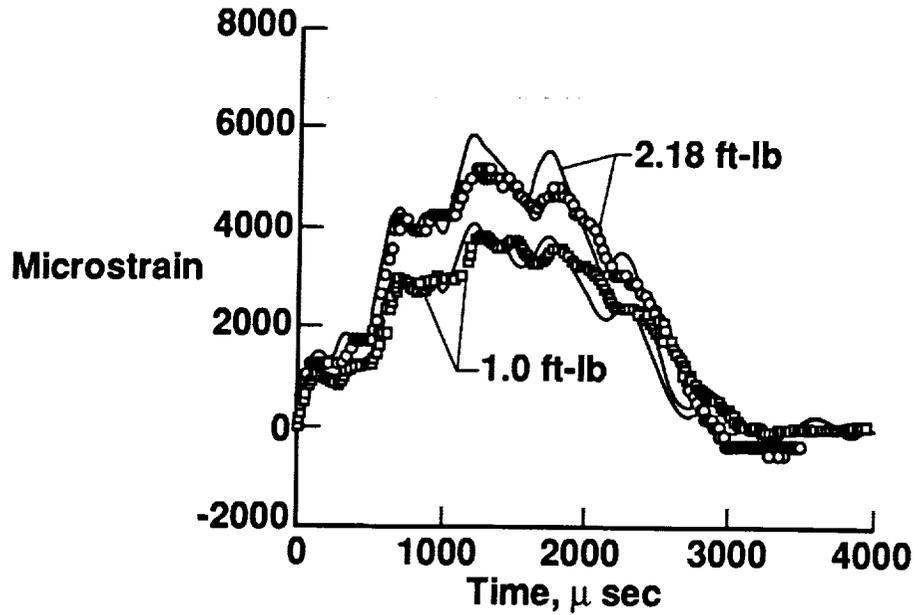
7(f) Comparison of analytical and experimental strains on surface opposite to impact side in a 32-ply simply supported laminated plate subjected to 1 and 2.18 ft-lb of dropped-weight impact.
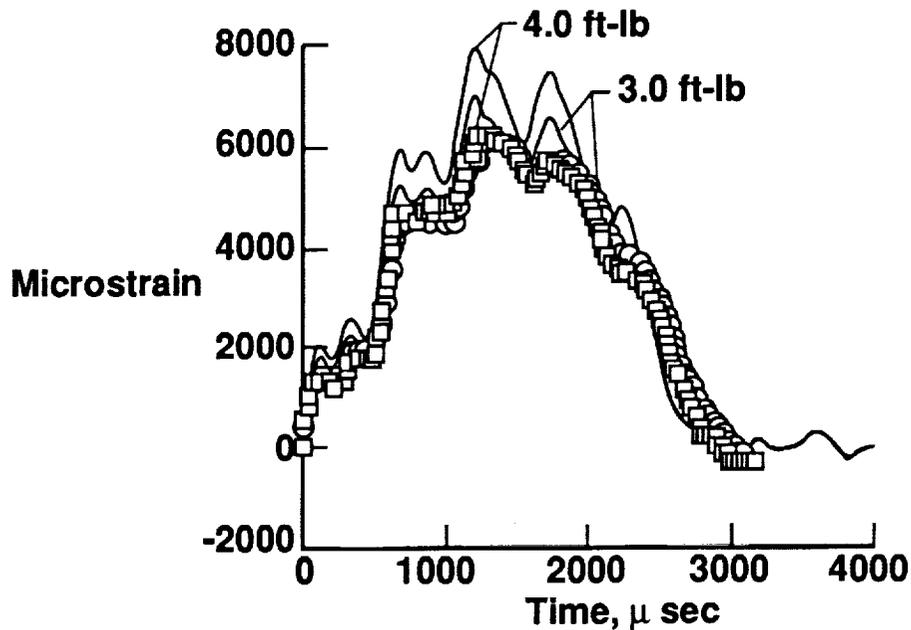
7(g) Comparison of analytical and experimental strains on surface opposite to impact side in a 32-ply simply supported laminated plate subjected to 3.0 and 4.0 ft-lb of dropped-weight impact.

Fig. 7 Concluded.
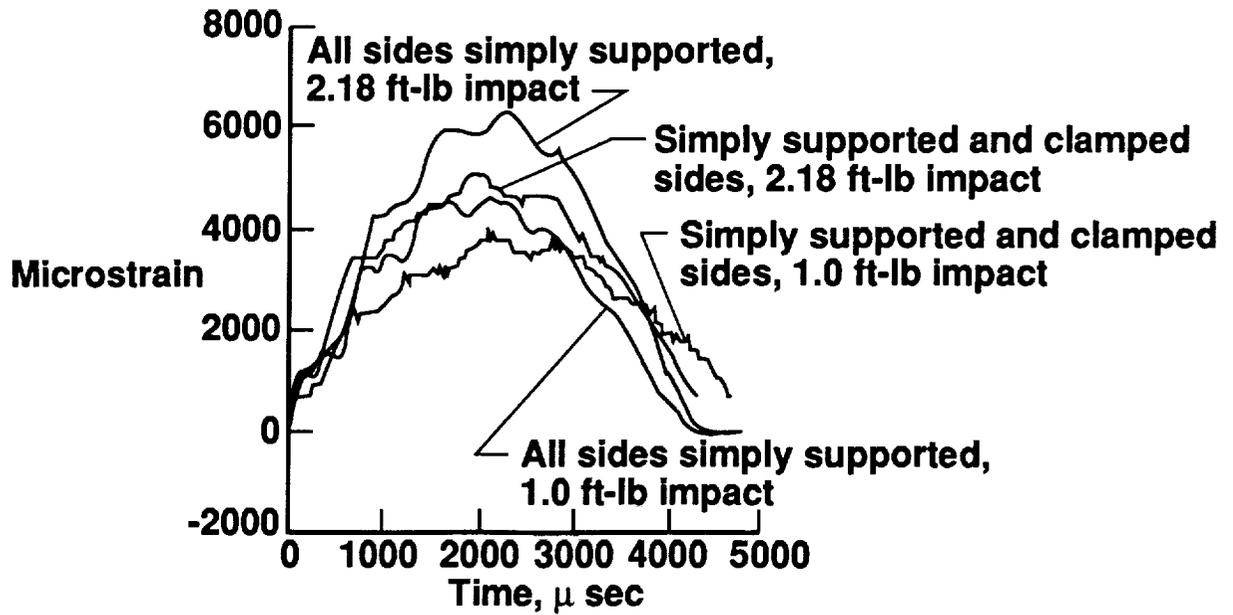
8(a) Comparison of measured strains on surface opposite to impact side in a 24-ply laminated plate with two different sets of boundary conditions subjected to dropped-weight impactors.

Fig. 8 Effect of boundary conditions and large deformations on the impact response of laminated graphite-epoxy plates.
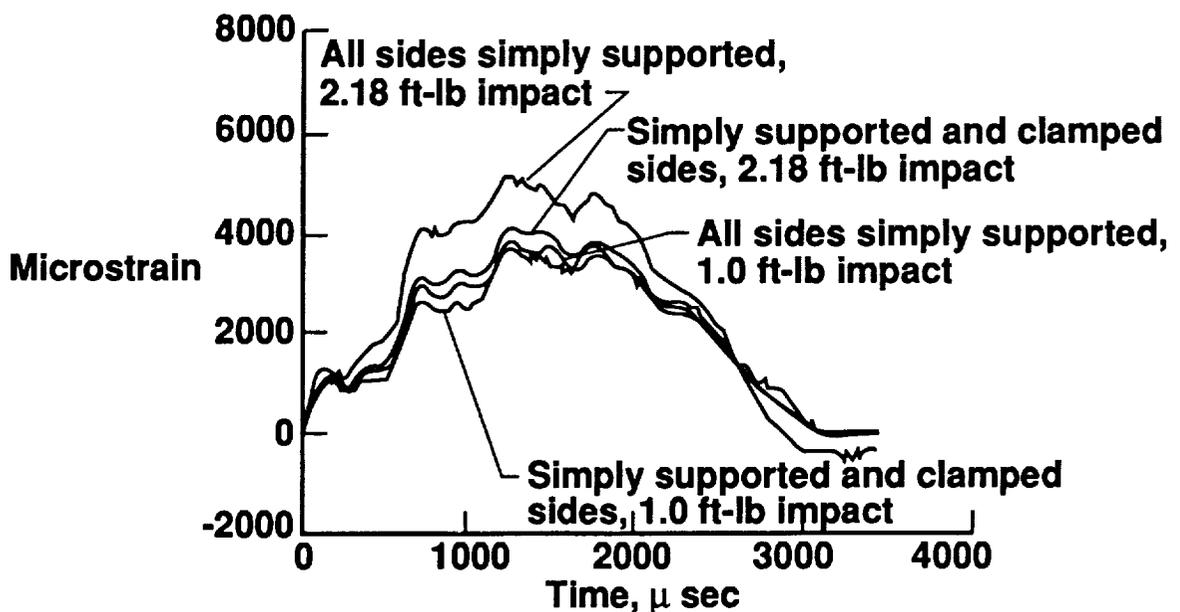
8(b) Comparison of measured strains on surface opposite to impact side in a 32-ply laminated plate with two different sets of boundary conditions subjected to dropped-weight impactors.

Fig. 8 Continued.
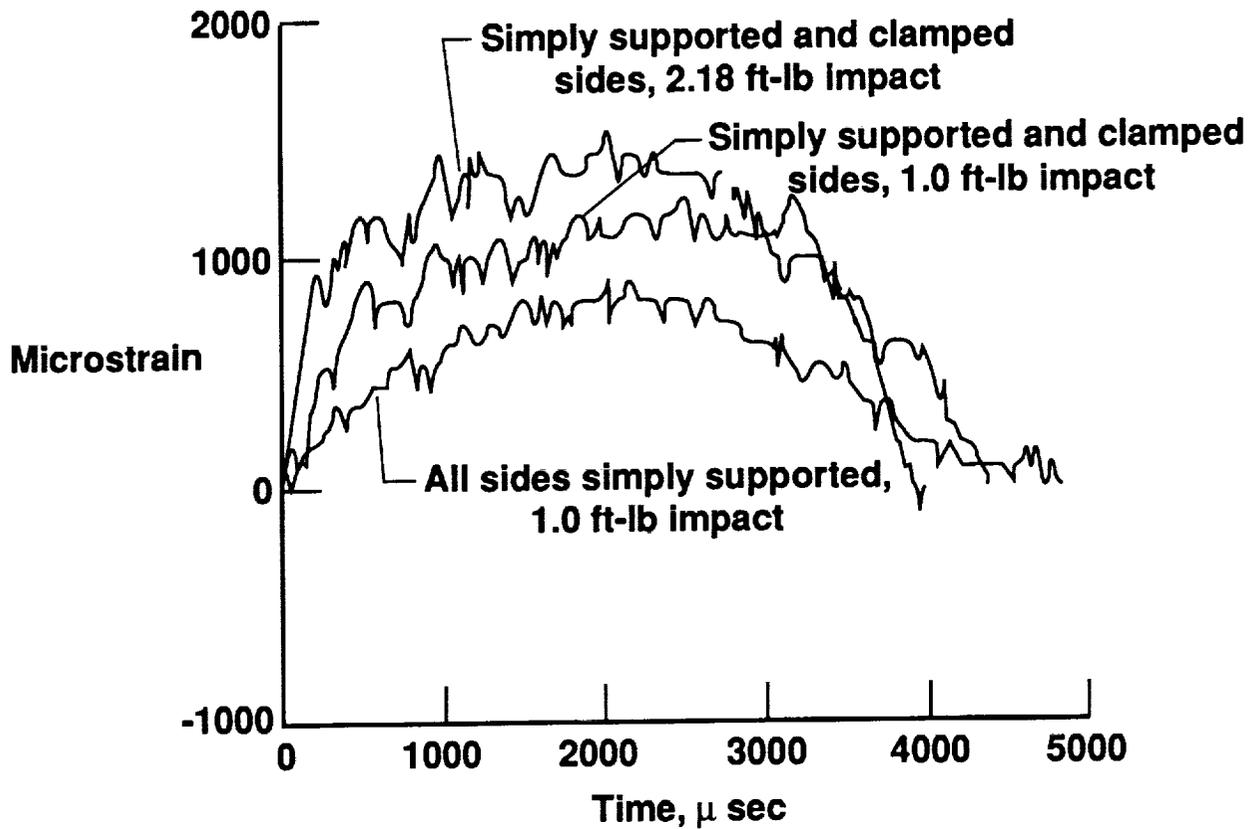
8(c) Comparison of measured membrane strains in a 24-ply laminated plate with two different sets of boundary conditions subjected to dropped-weight impactors.

Fig. 8 Concluded.

REPORT DOCUMENTATION PAGE

1. AGENCY USE ONLY *(Leave blank)*	2. REPORT DATE April 1993	3. REPORT TYPE AND DATES COVERED Technical Memorandum

4. TITLE AND SUBTITLE

Influence of Transverse-Shear and Large-Deformation Effects on the Low-Speed Impact Response of Laminated Composite Plates

5. FUNDING NUMBERS

WU 505-63-50-08

6. AUTHOR(S)

Damodar R. Ambur, James H. Starnes, Jr., and Chunchu B. Prasad

7. PERFORMING ORGANIZATION NAME(S) AND ADDRESS(ES)

NASA Langley Research Center
Hampton, VA 23681-0001

8. PERFORMING ORGANIZATION REPORT NUMBER

9. SPONSORING/MONITORING AGENCY NAME(S) AND ADDRESS(ES)

National Aeronautics and Space Administration
Washington, DC 20546-0001

10. SPONSORING/MONITORING AGENCY REPORT NUMBER

NASA TM-107753

11. SUPPLEMENTARY NOTES

Ambur and Starnes: Langley Research Center, Hampton, VA; Prasad: Analytical Services & Materials, Inc., Hampton, VA.

12a. DISTRIBUTION/AVAILABILITY STATEMENT

Unclassified - Unlimited

Subject Category - 24

12b. DISTRIBUTION CODE

13. ABSTRACT *(Maximum 200 words)*

An analytical procedure is presented for determining the transient response of simply supported, rectangular laminated composite plates subjected to impact loads from airgun-propelled or dropped-weight impactors. A first-order shear deformation theory is included in the analysis to represent properly any local-short-wave length transient bending response. The impact force is modeled as a locally distributed load with a cosine-cosine distribution. A double Fourier series expansion and the Timoshenko small-increment method are used to determine the contact force, out-of-plane deflections, and in-plane strains and stresses at any plate location due to an impact force at any plate location. The results of experimental and analytical studies are compared for quasi-isotropic laminates. The results indicate that using the appropriate local force distribution for the locally loaded area and including transverse-shear-deformation effects in the laminated plate response analysis are important. The applicability of the present analytical procedure based on small-deformation theory is investigated by comparing analytical and experimental results for combinations of quasi-isotropic laminate thicknesses and impact energy levels. The results of this study indicate that large-deformation effects influence the response of both 24- and 32-ply laminated plates and that a geometrically nonlinear analysis is required for predicting the response accurately.

14. SUBJECT TERMS

composite plate analysis; low-speed impact; transverse-shear effects; large-deformation effects; airgun and dropped-weight impactors

15. NUMBER OF PAGES

31

16. PRICE CODE

A03

17. SECURITY CLASSIFICATION OF REPORT	18. SECURITY CLASSIFICATION OF THIS PAGE	19. SECURITY CLASSIFICATION OF ABSTRACT	20. LIMITATION OF ABSTRACT
Unclassified	Unclassified	Unclassified	